Modeling the Rovibrationally Excited C_2H_4OH Radicals from the Photodissociation of 2-Bromoethanol at 193 nm

B. J. Ratliff,[†] C. C. Womack,[†] X. N. Tang,[†] W. M. Landau,[†] L. J. Butler,*[,†] and D. E. Szpunar*[,‡]

Department of Chemistry and the James Franck Institute, University of Chicago, Chicago, Illinois 60637, and Department of Biological, Chemical, and Physical Sciences, Roosevelt University, Schaumburg, Illinois 60173

Received: December 11, 2009; Revised Manuscript Received: February 19, 2010

This study photolytically generates, from 2-bromoethanol photodissociation, the 2-hydroxyethyl radical intermediate of the OH + ethene reaction and measures the velocity distribution of the stable radicals. We introduce an impulsive model to characterize the partitioning of internal energy in the C_2H_4OH fragment. It accounts for zero-point and thermal vibrational motion to determine the vibrational energy distribution of the nascent C_2H_4OH radicals and the distribution of total angular momentum, *J*, as a function of the total recoil kinetic energy imparted in the photodissociation. We render this system useful for the study of the subsequent dissociation of the 2-hydroxyethyl radical to the possible asymptotic channels of the OH + ethene reaction. The competition between these channels depends on the internal energy and the *J* distribution of the radicals. First, we use velocity map imaging to separately resolve the $C_2H_4OH + Br(^2P_{3/2})$ and $C_2H_4OH + Br(^2P_{1/2})$ photodissociation channels, allowing us to account for the 10.54 kcal/mol partitioned to the $Br(^2P_{1/2})$ cofragment. We determine an improved resonance enhanced multiphoton ionization (REMPI) line strength for the Br transitions at 233.681 nm ($5p\ ^4P_{1/2} \leftarrow 4p\ ^2P_{3/2}$) and 234.021 nm ($5p\ ^2S_{1/2} \leftarrow 4p\ ^2P_{1/2}$) and obtain a spin−orbit branching ratio for $Br(^2P_{1/2})$:$Br(^2P_{3/2})$ of 0.26 ± 0.03:1. Energy and momentum conservation give the distribution of total internal energy, rotational and vibrational, in the C_2H_4OH radicals. Then, using 10.5 eV photoionization, we measure the velocity distribution of the radicals that are stable to subsequent dissociation. The onset of dissociation occurs at internal energies much higher than those predicted by theoretical methods and reflects the significant amount of rotational energy imparted to the C_2H_4OH photofragment. Instead of estimating the mean rotational energy with an impulsive model from the equilibrium geometry of 2-bromoethanol, our model explicitly includes weighting over geometries across the quantum wave function with zero, one, and two quanta in the harmonic mode that most strongly alters the exit impact parameter. The model gives a nearly perfect prediction of the measured velocity distribution of stable radicals near the dissociation onset using a G4 prediction of the C−Br bond energy and the dissociation barrier for the OH + ethene channel calculated by Senosiain et al. (*J. Phys. Chem. A* **2006**, *110*, 6960). The model also indicates that the excited state dissociation proceeds primarily from a conformer of 2-bromoethanol that is trans across the C−C bond. We discuss the possible extensions of our model and the effect of the radical intermediate's *J*-distribution on the branching between the OH + ethene product channels.

I. Introduction

The reaction of OH with ethene is of great importance in both combustion processes and atmospheric chemistry. Recent studies conclude that this bimolecular reaction is the dominant source of ethenol in many flames including those of allene, ethanol, and ethene.[1−3] Additionally, alkenes are an important class of volatile organic compounds and their atmospheric oxidation occurs primarily via reaction with OH.[4] For these reasons, the OH + ethene reaction has received considerable attention in both theoretical[5−19] and experimental work.[20−65]

The reaction of OH with ethene may proceed via direct H abstraction to form $H_2O + CHCH_2$ or undergo an addition reaction to form the 2-hydroxyethyl radical intermediate. Early studies[36,41,49] measured the rate constant as a function of temperature and pressure. At high temperatures the direct H atom abstraction channel to form H_2O + vinyl plays an important role. Tully[41,49] concluded that the reaction at low temperatures is dominated by the addition of the OH to the double bond, but that the reaction intermediate primarily redecomposes to OH + ethene instead of branching to one or more of the energetically allowed product channels. Subsequent master equation modeling[62,63] supported this conclusion, although those studies neglected to include a possible H + ethenol product channel in the model. Two studies[64,65] have aimed to experimentally determine product yields of the OH + C_2H_4 reaction. One[64] reported the temperature dependence of the high-pressure limiting rate coefficients and the pressure dependent yield of $CH_3 + CH_2O$ at high pressures, while the other study[65] at 2 Torr of He and 295 K determined that the OH + ethene products consisted of 21% stabilized C_2H_4OH adduct, 44% formaldehyde, and 35% C_2H_4O, attributed to acetaldehyde. Flame studies[2,3] that detect an ethenol product channel from the reaction of OH + ethene have generated renewed interest in the reaction dynamics. Recent theoretical work[19] has considered the possible competition between several isomerization and decomposition pathways of the C_2H_4OH radical intermediate

* Authors to whom correspondence should be addressed. Electronic addresses: L.J.B., L-Butler@uchicago.edu; D.E.S., DSzpunar@roosevelt.edu.
[†] University of Chicago.
[‡] Roosevelt University.

10.1021/jp911739a
Published on Web 03/19/2010

formed in the addition mechanism, including H + ethenol. According to the calculated potential energy surface,[19] the C_2H_4OH radical may redisocciate to OH + ethene, undergo direct C−H bond fission to form H + ethenol, or isomerize to the ethoxy radical and undergo either C−C bond fission to form CH_3 + formaldehyde or C−H bond fission to form H + acetaldehyde. The study presented here focuses on generating the C_2H_4OH radical intermediate photolytically with a well-characterized distribution of rotational and vibrational energies, which allows subsequent studies of the microcanonical branching to the competing product channels of the OH + ethene reaction.

Our method for studying the dynamics of bimolecular reactions starts with a photolytic precursor to create a radical intermediate on the potential energy surface with a range of internal energies. Several experiments have focused on the photodissociation dynamics of the 2-haloethanols, which are possible precursors for the 2-hydroxyethyl intermediate on the OH + ethene potential energy surface.[58−61] Two of the 2-haloethanols, 2-chloroethanol and 2-iodoethanol, are not suitable precursors for accessing the OH + ethene potential energy surface. The low absorption cross-section of 2-chloroethanol at 193 nm results in insufficient C_2H_4OH signal.[58] The photodissociation of 2-iodoethanol[59,61] at 266 nm results in C_2H_4OH photofragments that are highly rotationally excited and thus stable to secondary dissociation to OH + C_2H_4. Additionally, some of the energetically stable C_2H_4OH radicals may photodissociate by absorbing an additional 266 nm photon. Pratt and co-workers[61] report a small preferential loss of the radicals that are momentum-matched to $I(^2P_{3/2})$ but are ultimately unable to ascertain whether the radicals are lost due to photodissociation, dissociative ionization, or secondary decomposition. In contrast, the photodissociation of 2-bromoethanol at 193 nm, while still partitioning a large amount of rotational energy to the C_2H_4OH radical, produces a substantial portion that can dissociate to OH + C_2H_4. Thus our work focuses on the precise characterization of the distribution of rotational and vibrational energy imparted to the C_2H_4OH radicals as a function of relative kinetic energy in the photodissociation of 2-bromoethanol at 193 nm. We review the key features of the prior experiments below.

The most relevant prior work on 2-bromoethanol photodissociation is that of Lee and co-workers[58] using a crossed laser molecular beam scattering apparatus with electron impact detection. They resolved the distribution of recoil kinetic energies imparted in C−Br bond fission and detected the velocity distribution of the subset of C_2H_4OH radicals formed stable to subsequent dissociation. They also detected the OH + C_2H_4 products from the C_2H_4OH radicals formed with higher internal energy. Although some of the stable C_2H_4OH radicals had internal energies well above the expected C_2H_4−OH bond energy if they were formed in conjunction with ground spin−orbit state Br atoms, $Br(^2P_{3/2})$, they noted that these radicals would be energetically stable if they had formed in conjunction with $Br(^2P_{1/2})$. Lee and co-workers also considered the possibility that the large exit impact parameter of the C−Br fission could result in rotationally metastable C_2H_4OH. This explanation agrees with the observation of a strongly forward−backward peaked angular distribution of the OH + C_2H_4 products from the unstable radicals. However, their detection method did not allow them to resolve the Br spin−orbit state. Thus they were unable to distinguish whether the radicals were stable due to high rotational energies or because 10.54 kcal/mol of energy was partitioned to the $Br(^2P_{1/2})$ cofragment. Subsequent work by Chandler et al.[59] in 1990 reported the selective detection of the $Br(^2P_{3/2})$ and $Br(^2P_{1/2})$ cofragments in an imaging experiment. Although Chandler et al. did not present the full recoil kinetic energy distribution for each Br spin−orbit state, they did note that the highest recoil velocity observed for $Br(^2P_{3/2})$ was slower than expected and attributed the difference to the high rotational energy imparted to the radical. In 1992, Sapers and Hess[60] used laser induced fluorescence to characterize the velocity, via Doppler measurement, and the internal state distribution of the OH products formed from the subsequent dissociation of the C_2H_4OH radicals. In their attempt to model the rotational distribution of the OH fragment they used a modified soft radical impulsive model to predict the rotational energy in the C_2H_4OH photofragment. Assuming the Br atom recoils impulsively from the $CH_{2,\beta}$ moiety, the model predicts that the C_2H_4OH radicals are formed with an average rotational energy of 144 kJ/mol with a $Br(^2P_{3/2})$ cofragment and 124 kJ/mol with a $Br(^2P_{1/2})$ cofragment.

Any impulsive model for predicting the J state distribution of radicals from a photodissociation event should, in principle, explicitly consider the distribution of conformers of the photolytic precursor. The rotational conformers of the 2-haloethanols have been studied by infrared spectroscopy,[66,67] electron diffraction,[68−72] and microwave spectroscopy.[73,74] We will refer to the conformers as the Tg, Gt, Gg, Gg′, and Tt conformers, where the first letter denotes "T" for trans and "G" for gauche about the C−C bond and the second letter denotes "t" for trans and "g" for gauche about the O−C bond. These conformers are depicted in the Supporting Information. Experiments and theory have concluded that the Gg conformer of 2-bromoethanol is lower in energy than the Tg and Tt conformers by over 1 kcal/mol due to a hydrogen bonding interaction between the Br and hydroxyl hydrogen. A study by Hedberg and co-workers[70] reported the rotameric composition of 2-bromoethanol in the gas phase at several temperatures, finding that 21.4% of conformers are trans about the C−C bond at 200 °C. For the work presented here, the key effect of conformation is that the exit impact parameter of C−Br dissociation is substantially larger for the gauche conformers about the C−C bond than for the trans conformers of 2-bromoethanol.

In this paper we offer a detailed model of the rotational and, by energy conservation, the vibrational energy distribution in the nascent C_2H_4OH radicals. We explicitly include in the model our measured recoil kinetic energy distributions for C_2H_4OH + $Br(^2P_{3/2})$ and C_2H_4OH + $Br(^2P_{1/2})$. This allows us to separately identify the contributions from energetically stable and rotationally metastable C_2H_4OH radicals in the measured kinetic energy distribution of the radicals that do not dissociate. Unlike prior models for rotational energy partitioning, our model incorporates explicit averaging over the distribution of exit impact parameters in the C−Br bond fission due to zero-point and thermal vibrational motion of the 2-bromoethanol precursor. We hope that this more detailed analysis of the rovibrational energy distribution of the C_2H_4OH radicals as a function of velocity will allow us to compare subsequent velocity resolved product branching measurements with the J dependent microcanonical rate constants for the product channels predicted from ab initio potential energy surfaces.[19]

II. Experimental Methods

This work uses a 2-D velocity map imaging apparatus, described previously,[75−78] to detect the velocity and angular distributions of Br atoms and stable C_2H_4OH radicals. Passing helium gas through a liquid sample of 2-bromoethanol (95% purity), maintained at 40 °C, created a molecular beam of 1.5%

2-bromoethanol. At a total stagnation pressure of 500 Torr, the molecular beam supersonically expanded through a heated General Valve Iota One pulsed valve with an orifice diameter of 0.8 mm and a temperature of 72 °C. After passing through a skimmer, the molecular beam crossed, at right angles, the polarized 193.3 nm photodissociation light from a GAM (EX10F/300) ArF laser. We use the vertically polarized component obtained by passing the unpolarized 193.3 nm output of the laser through a single crystal quartz birefringent Pellin-Broca. The lens that focused the vertically polarized 8 mm by 4 mm beam had a focal length of 250 mm and a focal point near the intersection with the molecular beam. Typical 193 nm pulse energies were 1 mJ/pulse. The photolysis laser fired 40 ns prior to the ionization laser.

We used 2+1 resonance-enhanced multiphoton ionization (REMPI) to state-selectively ionize the $Br(^2P_{3/2})$ and $Br(^2P_{1/2})$ photofragments with 233.681 nm ($5p\ ^4P_{1/2} \leftarrow 4p\ ^2P_{3/2}$) and 234.021 nm ($5p\ ^2S_{1/2} \leftarrow 4p\ ^2P_{1/2}$) photons, respectively. Tripling the output of a Lambda Physik, FL 3002 dye laser (LDS 698 dye) pumped by an injection-seeded Nd:YAG laser (Continuum Powerlite Precision 9020) generated these REMPI wavelengths. The ~702 nm dye laser output passed through a potassium dihydrogen phosphate crystal, doubling the frequency, and then mixed with the fundamental in a β-barium borate crystal to produce vertically polarized photons at the REMPI wavelength. After tightly focusing with a 25.4 cm focusing lens, this light crossed the molecular beam at a right angle in the main chamber of the imaging apparatus. We attenuated the laser pulse energy to minimize the Coulombic repulsion between the ionized fragments.

We determine the spin−orbit branching ratio, $N[Br(^2P_{1/2})]/N[Br(^2P_{3/2})]$, by integrating the total ion signal from Br atoms in each spin−orbit state, $S[Br(^2P_{1/2})]$ and $S[Br(^2P_{3/2})]$, in images accumulated while scanning the Doppler profiles ±0.008 nm from line center and weighting this result by the REMPI line strength, k:

$$\frac{N[Br(^2P_{1/2})]}{N[Br(^2P_{3/2})]} = k\frac{S[Br(^2P_{1/2})]}{S[Br(^2P_{3/2})]} \quad (1)$$

Lau et al.[79] previously reported the REMPI line strength, k, for the 233.681 nm ($5p\ ^4P_{1/2} \leftarrow 4p\ ^2P_{3/2}$) and 234.021 nm ($5p\ ^2S_{1/2} \leftarrow 4p\ ^2P_{1/2}$) transitions to be 0.17 ± 0.05, but here we adopt a revised value of $k = 0.32 \pm 0.02$. Both determinations begin by measuring the relative signal intensities for the $Br(^2P_{1/2})$ and $Br(^2P_{3/2})$ photofragments from the 234 nm photodissociation of 1-bromo-2-butene and then changing the value of k in eq 1 to reproduce the spin−orbit branching ratio of 2.03 ± 0.05:1 for $Br(^2P_{1/2})$:$Br(^2P_{3/2})$. (The total recoil kinetic energy distribution, $P(E_T)$, calculated using this spin−orbit branching ratio correctly matches the $P(E_T)$ determined from the 1-methylallyl radical cofragments when the individual measured $Br(^2P_{1/2})$ and $Br(^2P_{3/2})$ velocity distributions are weighted and summed.) The prior work[79] measured the relative ion signal for $Br(^2P_{1/2})$ and $Br(^2P_{3/2})$ of 12.27:1 by integrating the time-of-flight profile for each Br spin−orbit state at the wavelength that maximized signal intensity. We could not reproduce this value, nor does it probe the entire Doppler profile of the Br photofragments. This method for measuring the relative ion signal is only accurate if the Doppler line shapes for the Br spin−orbit states are identical. Thus, here we refine the REMPI line strength for the ($5p\ ^4P_{1/2} \leftarrow 4p\ ^2P_{3/2}$) and ($5p\ ^2S_{1/2} \leftarrow 4p\ ^2P_{1/2}$) transitions by measuring the relative the signal intensities for the $Br(^2P_{1/2})$ and $Br(^2P_{3/2})$ photofragments resulting from the 234 nm photodissociation of 1-bromo-2-butene by integrating the ion intensity on images accumulated while scanning the entire Doppler profile ±0.008 nm from line center. Six trials gave a $S[Br(^2P_{1/2})]/S[Br(^2P_{3/2})]$ value of 6.3 ± 0.4 (95% confidence interval) resulting in a revised REMPI line strength of $k = 0.32 \pm 0.02$, double that determined by Lau et al.

We detected the C_2H_4OH radical products with single photon ionization at 118 nm, generated by tripling the 355 nm output of a pulsed Nd:YAG laser (Continuum Surelite I-20). The 355 nm light passed through a beam expander (focal length = −150 mm and focal length = 300 mm at 588 nm) and then two lenses to focus the light into a 21 cm low-pressure gas cell filled with 25 Torr of high purity Xe (>99.995%). The gas cell, mounted on the main vacuum chamber, ends with a MgF_2 lens (focal length = 120.3 mm at 193 nm) that served as the barrier between the cell and the chamber. This lens recollimated the 355 nm light while softly focusing the 118 nm light. This arrangement generated some background counts from the 355 nm light hitting the ion optics.

Following photodissociation and photoionization, the electrostatic lens optics with repeller and extractor voltages in a ratio of 1.404:1 (2000 and 1424 V for Br atoms and 3932 and 2800 V for the detection of C_2H_4OH) accelerated the spherically expanding ions down a ~577 mm grounded time-of-flight tube toward the detector. The Burle 3040FM detector is a position sensitive Chevron microchannel plate (MCP) assembly coupled to a P20 phosphor screen. An 80 ns, −750 V pulse on the front plate of the MCP gates the ions based on arrival time. A cooled charge-coupled device (CCD) camera (La Vision Imager 3) with a standard 35 mm lens recorded the images of the ions appearing on the phosphor screen, which remained at 3.3 kV above the potential of the rear MCP plate. We use Houston's ion-counting method[80] to process the collected images. A digital delay pulse generator (Stanford Research DG535) controlled the timing sequence for opening the pulsed valve, firing the lasers, gating the MCP gain, and capturing the ion images at a repetition rate of 20 Hz.

III. G4 Calculations for 2-Bromoethanol

To help characterize 2-bromoethanol as a photolytic precursor to the 2-hydroxyethyl radical, we calculate the relative energetics of 2-bromoethanol's five distinct conformers and their respective C−Br bond dissociation energies. Optimized molecular geometries and vibrational frequencies of the CH_2BrCH_2OH conformers were found using the B3LYP density functional and the 6-311++G(3df,2p) basis set. The geometries converged to a root-mean-square (rms) force below 1×10^{-5} and an rms displacement below 4×10^{-5}, where both are in atomic units. Wave functions for doublet species were spin-unrestricted and wave functions for singlet species were spin-restricted. The computation of the zero-point vibrational energies used the B3LYP/6-311++G(3df,2p) vibrational frequencies scaled by 0.9854, as Curtiss et al. recommended[81] and the G4 method required.[82] The G4 method is the latest in the series of G*n* methods, which are composite methods based on a sequence of single point energy calculations. Table 1 presents the zero-point corrected G4 energies both at 0 K and the nozzle temperature of 345.15 K. The calculation of the C−Br bond dissociation energy also used the G4 method, where the dissociation energy D_0 is energy difference between each 2-bromoethanol conformer and the lowest energy conformer of the 2-hydroxyethyl radical + $Br(^2P_{3/2})$. The calculations use the Gaussian 09 Program, version A.02.[83] The Supporting Informa-

TABLE 1: Calculated C−Br Bond Energies of 2-Bromoethanol Conformers and the Resulting Available Energies for 193 nm Photodissociation

	D_0(C−Br)[a]	$E_{int}(CH_2BrCH_2OH)$[b]	$E_{avail} = E_{h\nu} + E_{int}(CH_2BrCH_2OH) - D_0$(C−Br)	E(0 K)[a]	E(345.15 K)[a]
Gt	68.54	2.14	81.40	1.98	6.18
Gg	70.52	1.94	79.22	0.00	4.00
Gg′	68.04	2.06	81.82	2.48	6.60
Tt	69.27	2.21	80.74	1.25	5.52
Tg	69.19	2.11	80.72	1.33	5.50

[a] Energies are calculated at the G4//B3LYP/6-311++G(3df,2p) level of theory and given in kcal/mol with the zero of energy set as the energy of the Gg conformer at 0 K. [b] The average internal energy of the photolytic precursor is calculated by assuming a thermal distribution at the nozzle temperature of 345.15 K. We use the harmonic vibrational frequencies calculated at the B3LYP/6-311++G(3df,2p) level and scaled by 0.9854.

tion gives all the relevant structures, harmonic vibrational frequencies, displacement vectors for motion along the harmonic vibrations, rotational constants, energies, and zero-point corrections.

IV. Results

The sections below describe our method to determine the rotational energy distribution of C_2H_4OH radicals formed from the photodissociation of 2-bromoethanol at 193 nm, some of which have sufficient vibrational energy to access both the OH + ethene reactant asymptote and the product channels accessed via the C_2H_4OH radical intermediate. We begin in section A by measuring the Br($^2P_{3/2}$) and Br($^2P_{1/2}$) velocity distributions and the Br($^2P_{3/2}$):Br($^2P_{1/2}$) spin−orbit branching ratio. We use momentum conservation to calculate the total recoil translational energy distribution, $P(E_T)$, for all C−Br bond fission events. Our measurement of the velocity distribution of the stable radicals, when compared to the $P(E_T)$ determined for all C−Br fission events in section A, shows that radicals formed with low recoil kinetic energies dissociate. In section B, we apply energy conservation to determine the internal energy distribution of the nascent C_2H_4OH radicals. Although our total internal energy distribution for the C_2H_4OH radicals shows that all of the radicals have internal energies above the lowest dissociation barrier, the one to OH + ethene, some of the radicals are energetically stable because a substantial fraction of the internal energy is partitioned to rotation rather than vibration. After presenting the velocity distribution of the stable C_2H_4OH radicals detected with 10.5 eV photoionization in section C, we evaluate an impulsive model for the rotational energy partitioning in section D. In this model, we consider the contributions from the different conformers of 2-bromethanol and, more importantly, their vibrational wave functions to obtain a vibrational energy distribution for the nascent radicals. We test this model for the partitioning of energy into rotational and vibrational energy by using it to predict the measured velocity distribution of the radicals that have low enough vibrational energy to be energetically stable. (i.e., the radicals with vibrational energy below the lowest dissociation channel, the OH + ethene reactant asymptote.) The excellent agreement between the model and our measured C_2H_4OH velocity distribution in the threshold region and the good agreement across the C_2H_4OH velocity distribution allows us to characterize the J distribution and the vibrational energy distribution of the nascent radicals as a function of their velocity. Such a characterization is necessary to interpret subsequent measurements of the internal energy dependent branching to the possible dissociation channels: the OH + ethene reactant asymptote, or the H + ethenol, H + acetaldehyde, and CH_2O + CH_3 product asymptotes of the bimolecular reaction of OH + ethene.

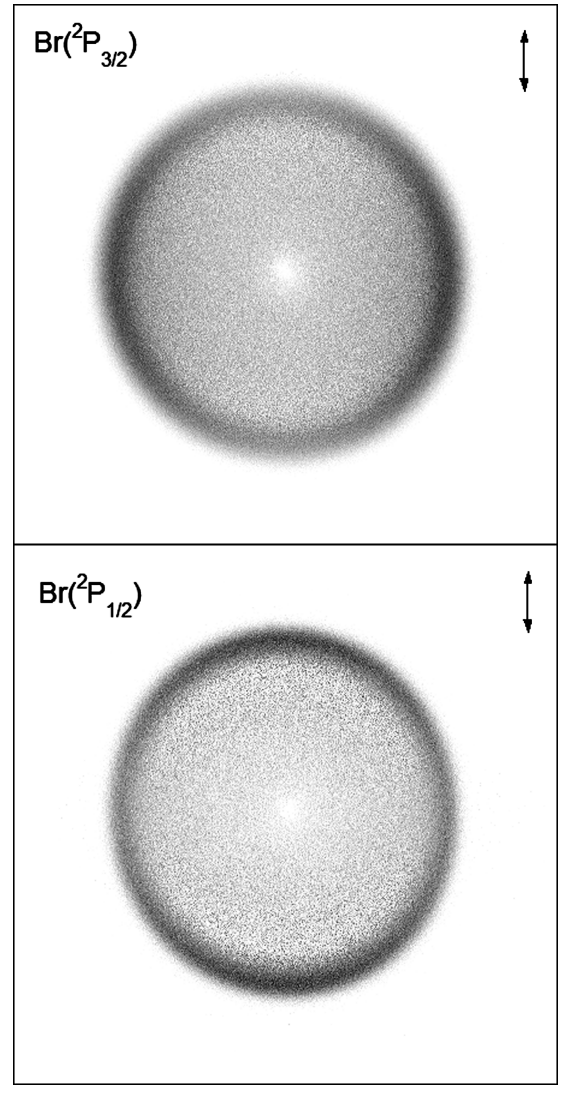

Figure 1. Images of Br($^2P_{3/2}$) and Br($^2P_{1/2}$) detected with 2+1 REMPI following the photodissociation of 2-bromoethanol at 193 nm. The photodissociation laser was polarized along the vertical plane of the image, as the arrows indicate. Each image is 901 × 901 pixels and was background subtracted by subtracting the images obtained with 193 nm only and 234 nm only from the raw data.

A. Translational Energy Distribution for C−Br Bond Fission. We determine the kinetic energy distribution for C−Br bond fission from 193.3 nm photodissociation of 2-bromoethanol by measuring the recoil velocities of the Br photofragments. Figure 1 shows the 2-dimensional ion images of Br($^2P_{3/2}$) and Br($^2P_{1/2}$) with the photodissociation laser polarized along the vertical axis; these images are background subtracted and show the signal resulting from 193.3 nm photodissociation and REMPI

TABLE 2: Anisotropy Parameters for the Br Photofragment Angular Distribution

	anisotropy parameters[a]
$Br(^2P_{3/2})$	$\beta_2 = -0.20$
	$\beta_4 = -0.05$
$Br(^2P_{1/2})$	$\beta = 0.58$

[a] The $Br(^2P_{3/2})$ angular distribution was fit to $1 + \beta P_2(\cos\theta)$ and the $Br(^2P_{1/2})$ angular distribution was fit to $1 + \beta_2 P_2(\cos\theta) + \beta_4 P_4(\cos\theta)$. In these equations, θ is the angle between the recoiling fragment's velocity and the electric vector of the photolysis laser, P_2 and P_4 are the second- and fourth-order Legendre polynomials, and β is the anisotropy parameter.

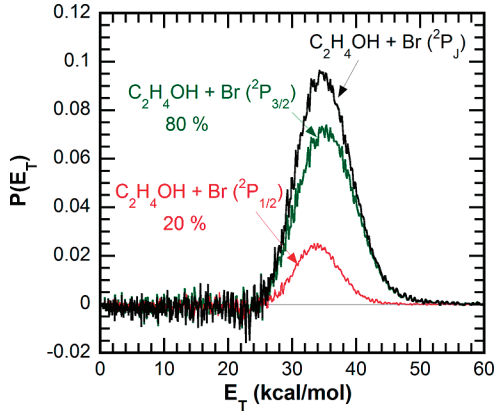

Figure 2. Normalized total recoil translational energy distribution for the C−Br bond photofission of 2-bromoethanol at 193 nm (black) which is a sum of the distributions obtained for $Br(^2P_{3/2}) + C_2H_4OH$ (green) and $Br(^2P_{1/2}) + C_2H_4OH$ (red), weighted by their spin−orbit branching ratio of 1:0.26 ± 0.03, respectively.

ionization. Table 2 gives the anisotropy parameters that fit the angular distributions apparent in these images. The Supporting Information presents figures and further analysis of these angular distributions. Each image is used to reconstruct the three-dimensional scattering distribution using an inverse Abel transformation in the BASEX Program.[84] Integrating the three-dimensional velocity distribution over all solid angles at each speed gives the speed distributions, $P_{Br}(v)$, for each Br spin−orbit state. Figure 2 shows the center of mass recoil translational energy distributions, $P(E_T)$, for $Br(^2P_{3/2}) + C_2H_4OH$ and $Br(^2P_{1/2}) + C_2H_4OH$, which result from the measured Br velocity distributions using momentum conservation and applying a Jacobian correction. The sum of these kinetic energy distributions, weighted by their spin−orbit branching ratio, gives the total recoil kinetic energy distribution for Br + all nascent C_2H_4OH radicals, which is also shown in Figure 2. We determine the spin−orbit branching ratio, $N[Br(^2P_{3/2})]/N[Br(^2P_{1/2})]$, by integrating the total ion signal from each Br spin−orbit state, $S[Br(^2P_{3/2})]$ and $S[Br(^2P_{1/2})]$, in images accumulated over the entire Doppler profile, as described in the section on Experimental Methods. We weight the measured signal ratio by the newly determined REMPI line strength, $k = 0.32 \pm 0.02$, as shown in eq 1. The average numbers of net ion counts per laser shot for $Br(^2P_{1/2})$ and $Br(^2P_{3/2})$ were 75 and 95, respectively, giving a spin−orbit branching ratio for $Br(^2P_{1/2})$: $Br(^2P_{3/2})$ of 0.26 ± 0.03:1. The 95% confidence interval resulted from eight independent trials. Our total translational energy distribution peaks at 35 kcal/mol and has an average translational energy $\langle E_T \rangle = 35.2$ kcal/mol, which is in good agreement with Lee and co-workers' $P(E_T)$ that peaked at 33 kcal/mol and had an average $\langle E_T \rangle = 33.8$ kcal/mol.[58] Moreover, the data here distinguish the fraction of dissociation events that result in

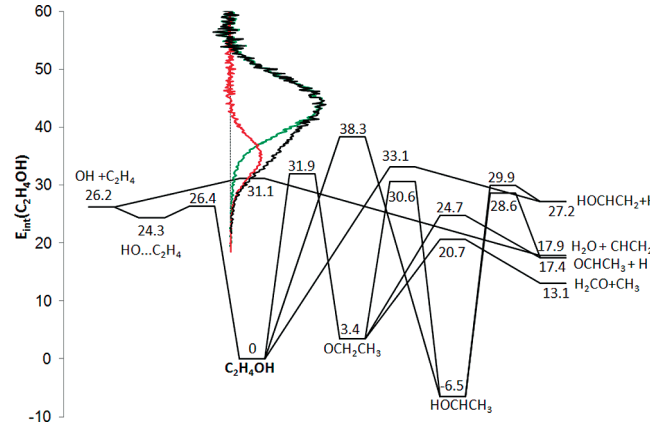

Figure 3. Internal energy distribution (solid black line), vibrational + rotational, of all nascent C_2H_4OH radicals resulting from the 193 nm photodissociation of 2-bromoethanol shown on the potential energy surface calculated by Senosiain et al.[19] (The internal energy distribution shown is calculated with the D_0(C−Br) for the Gg conformer.) The internal energy distribution for C_2H_4OH radicals formed in conjunction with $Br(^2P_{3/2})$ is shown by a green line, and the distribution for C_2H_4OH radicals formed in conjunction with $Br(^2P_{1/2})$ is shown as a red line.

$Br(^2P_{1/2})$ versus $Br(^2P_{3/2})$, which allows us to resolve the internal energy distribution of nascent C_2H_4OH radicals from our measured recoil translational energy distribution.

B. Internal Energy Distribution of Nascent C_2H_4OH Radicals. Using energy conservation and our measured translational energy distribution, we calculate the internal energy, rotational plus vibrational, of the nascent 2-hydroxyethyl radicals, $E_{int}(C_2H_4OH)$, from the following equation:

$$E_{int}(C_2H_4OH) = E_{h\nu} + E_{int}(CH_2BrCH_2OH) - D_0(C-Br) - E_{int}(Br(^2P_J)) - E_T \quad (2)$$

$E_{h\nu}$ is the energy of the 193.3 nm photodissociation photon, 147.8 kcal/mol. We assume that the supersonic expansion rotationally cools the parent 2-bromoethanol molecules and that they have a thermal distribution of vibrational energy at the nozzle temperature, 72 °C. Using the harmonic vibrational frequencies calculated at the B3LYP/6-311++G(3df,2p) level and scaled by 0.9854, we calculate the average internal energy, $E_{int}(CH_2BrCH_2OH)$, for the five conformers of 2-bromoethanol. Table 1 shows these values along with the respective G4(0K) energies, G4(345.15K) energies, G4//B3LYP/6-311++G(3df,2p) C−Br bond dissociation energies, D_0(C−Br), and the energy available, E_{avail}, to partition between the product's recoil translational energy and internal energy. The internal energy in each Br spin−orbit state, $Br(^2P_{3/2})$ and $Br(^2P_{1/2})$ is 0 and 10.54 kcal/mol, respectively.[85] The Gg conformer of 2-bromoethanol is the lowest in energy and the G4 energies at the nozzle temperature of 345.15 K predict that this conformer should account for 78% of the 2-bromoethanol molecules in the molecular beam. However, the impulsive model analysis in section D suggests that the majority of the conformers that are gauche about the C−C bond isomerize to a trans configuration in the excited state dissociation. Using the energetics calculated for the Gg conformer, we plot in Figure 3 the resulting internal energy distribution of the nascent radicals superimposed on the critical points of the OH + ethene potential energy surface calculated by Klippenstein et al.[19] All of the 2-hydroxyethyl radicals are formed with internal energies exceeding the lowest energy barrier height of 26.4 kcal/mol to OH + C_2H_4. The

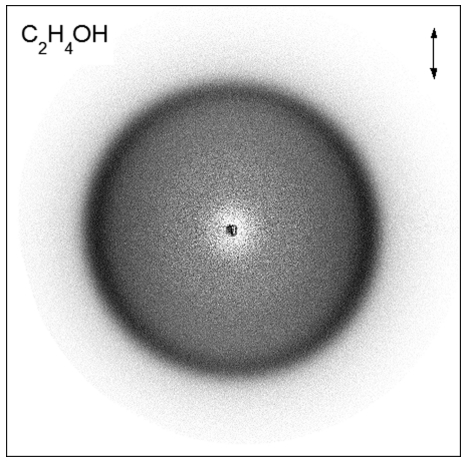

Figure 4. Image of the $m/e = 45$ signal containing the stable C_2H_4OH radicals. It was obtained with 118 nm photoionization following 193 nm photodissociation of 2-bromoethanol. The photodissociation laser was polarized in the vertical plane of the image, as shown with the arrow. The image is 901 pixels × 901 pixels and is the result of subtracting the background images obtained with 193 nm only and 118 nm only from the raw data.

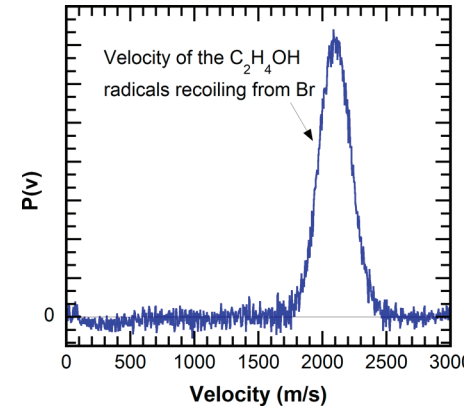

Figure 5. Background subtracted velocity distribution of the stable C_2H_4OH radicals. After the velocity distributions corresponding to the background images taken with 118 nm only and 193 nm only are subtracted from the raw data, the resulting $P(v)$ (shown in the Supporting Information) contains an underlying Gaussian-shaped distribution. This Gaussian-shaped background has been subtracted in the figure. The velocity distribution shown was used to calculate the $P(E_T)$ for Br + stable C_2H_4OH radicals, which is shown in frame a of Figure 6.

detection of energetically stable 2-hydroxyethyl radicals described below is consistent with previous work that concluded that a significant portion of the radical's internal energy is partitioned into rotational energy, the latter of which does not contribute to surmounting the dissociation and isomerization barriers.

C. Detection of Energetically Stable C_2H_4OH Radicals. Ionization and detection of the 2-hydroxyethyl radicals provide a measurement of the total recoil kinetic energy distribution for photodissociation events that result in energetically stable radicals. We use 118 nm (10.5 eV) photoionization to detect the stable 2-hydroxyethyl radicals giving the two-dimensional ion image in Figure 4. This background subtracted image shows the signal resulting from 193.3 nm photodissociation and subsequent 118 nm photoionization. The Supporting Information presents an analysis of the angular distribution. The recoil velocity distribution corresponding to the image in Figure 4 is shown in the Supporting Information and was reproducible over three separate days spanning several months. The velocity distribution contains a distinct underlying background due to the laser light hitting the ion optics. Removing this background entailed fitting a Gaussian curve to the data and subtracting it out. The resulting $P(v)$ shown in Figure 5 was then used to calculate the portion of the total $P(E_T)$ that corresponds to the formation of Br + energetically stable C_2H_4OH radicals, as shown in frame a of Figure 6. These stable C_2H_4OH radicals are those with vibrational energy below the OH + ethene dissociation barrier; they include both those with lower vibrational energy because 10.54 kcal/mol was partitioned to the $Br(^2P_{1/2})$ cofragment and those with lower vibrational energy because significant energy was partitioned to product rotation. (Lee and co-workers referred to this second group as metastable radicals.) The modeling that section D describes separately identifies these two sources of stability. The 2-hydroxyethyl radicals are momentum-matched to both ^{79}Br and ^{81}Br, which have an isotopic abundance of 0.507:0.493; we treat the radicals as if they were momentum-matched to an average mass of 80. (Our previous work on chlorinated species[86,87] used a more accurate forward convolution method to account for momentum conservation with each halogen isotope. This proved to have a negligible effect on the $P(E_T)$ determined here.) Our $P(E_T)$ for the production of energetically stable radicals peaks at 37 kcal/

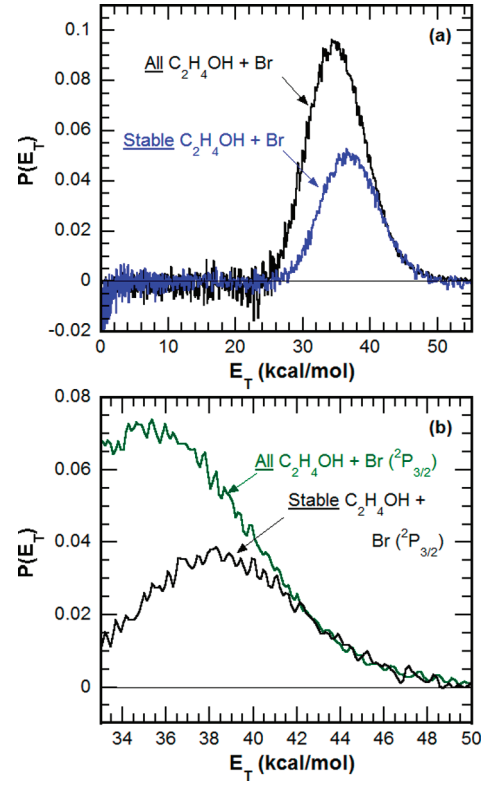

Figure 6. (a) Comparison of the $P(E_T)$ for the production of Br + all nascent C_2H_4OH radicals (black) to the $P(E_T)$ for the production of Br + energetically stable C_2H_4OH radicals (blue). (b) Comparison of the $P(E_T)$ for the production of all $Br(^2P_{3/2})$ + C_2H_4OH radicals (green) to the $P(E_T)$ for the production of $Br(^2P_{3/2})$ + energetically stable C_2H_4OH radicals (black).

mol and has an $\langle E_T \rangle = 36.9$ kcal/mol, in good agreement with the $P(E_T)$ determined by Lee's group, which peaked at 36 kcal/mol and had an $\langle E_T \rangle$ of 36.1 kcal/mol. The distributions differ on the low kinetic energy side, likely because the expansion conditions are different.

Frame a of Figure 6 compares the total recoil kinetic energy distribution obtained from all C−Br photodissociation events to the $P(E_T)$ for the production of stable radicals. At high translational energies, which correspond to low internal energies,

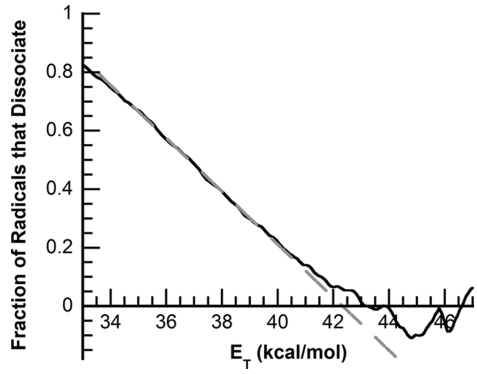

Figure 7. Fraction of the nascent C_2H_4OH radicals formed with the $Br(^2P_{3/2})$ cofragment that undergo dissociation (black solid line) shown as a function of the $Br(^2P_{3/2}) + C_2H_4OH$ total recoil translational energy. The *x*-intercept of the linear fit to the data between 35−40 kcal/mol (gray dashed line) gives a threshold E_T for C_2H_4OH dissociation of 42 ± 2 kcal/mol.

the radicals do not have sufficient vibrational energy to dissociate. Therefore, the $P(E_T)$s match in that region. However, at recoil energies less than 42 kcal/mol, some of the radicals have enough vibrational energy to surmount the barrier for dissociation to OH + ethene. At a given total recoil translational energy, C_2H_4OH radicals that form in conjunction with $Br(^2P_{1/2})$ have 10.54 kcal/mol less internal energy than those formed in conjunction with $Br(^2P_{3/2})$. Therefore, for C−Br bond fission events that impart more than 32 kcal/mol to recoil kinetic energy, only radicals formed in conjunction with $Br(^2P_{3/2})$ may dissociate. To analyze the onset of radical dissociation in frame b of Figure 6, we plot the $P(E_T)$ for all photodissociation events that formed $Br(^2P_{3/2}) + C_2H_4OH$ against the $P(E_T)$ for the formation of $Br(^2P_{3/2})$ + stable C_2H_4OH radicals. Note that radicals produced in conjunction with $Br(^2P_{1/2})$ atoms with E_T > 32 kcal/mol are stable; the corresponding $P(E_T)$ is shown in red in Figure 2. Thus we subtract this distribution from the $P(E_T)$ for all stable radicals + Br to calculate the $P(E_T)$ for the production of $Br(^2P_{3/2})$ + stable C_2H_4OH radicals shown in Figure 6b. We then determine an empirical dissociation threshold. Figure 7 shows the percent of radicals formed in conjunction with $Br(^2P_{3/2})$ that dissociate as a function of the recoil translational energy. A linear fit to the data between 35 and 40 kcal/mol gives an empirical kinetic energy threshold of 42 ± 2 kcal/mol, which is in good agreement with Lee's threshold kinetic energy of 39 kcal/mol. Using energy conservation (eq 2), this threshold E_T corresponds to 2-hydroxyethyl radicals formed with a total internal energy of 39.6 kcal/mol. Clearly this is well above the theoretical dissociation barrier to OH + ethene, so the entire distribution of radicals must have significant rotational energy (as one would expect from dissociation along the C−Br bond on a repulsive excited state accessed at 193 nm). The data show a small fraction of stable 2-hydroxyethyl radicals even down to $E_T = 28$ kcal/mol, which corresponds to an $E_{int} = 52.6$ kcal/mol. From our measured velocity distribution of $Br(^2P_{1/2})$ and the corresponding $P(E_T)$ in Figure 2, we know that for some radicals 10.54 kcal/mol is partitioned to the spin−orbit excitation of the Br atom cofragment. However, this does not account for the energetic stability of a significant percentage of the nascent radicals. The next section presents a detailed model for the rotational energy partitioning that captures the energetic onset of the loss of radicals as well as the large range of recoil kinetic energies over which some but not all radicals survive dissociation.

D. Impulsive Model for the Rotational Energy Partitioning.

D.1. Using an Impulsive Model to Derive the Rotational Energy Distribution of Nascent C_2H_4OH Radicals. While simple impulsive models such as the hard and soft radical impulsive models have been used to estimate the amount of energy partitioned to rotation and translation in photodissociation experiments, this section presents a more detailed model for the angular momentum partitioned to the photofragments in this experiment. The model begins with the measured distribution of recoil kinetic energies, rather than estimating a recoil kinetic energy with a simple hard or soft radical approximation.[60,88] Then it invokes conservation of angular momentum to determine the angular momentum imparted to the radical product for each measured E_T. We introduce a key refinement by making the prediction not just for the equilibrium geometry of the molecule[89] but rather for all the geometries the molecule accesses as it vibrates along its zero-point level (and later, in quantum states with quanta in the modes of importance for the rotational energy partitioning). We validate this model in section D.3 by using our predicted rotational energy distribution to predict the $P(E_T)$ for stable C_2H_4OH radicals and comparing it to our experimentally measured stable C_2H_4OH radical $P(E_T)$.

Our model for the rotational energy partitioning to nascent radicals begins with a classical model for angular momentum conservation. We neglect both the angular momentum of the photon and the electronic angular momentum of the products and assume that the supersonic expansion rotationally cools the 2-bromoethanol molecule, so that its initial angular momentum is zero. Conservation of angular momentum then requires that the classical orbital angular momentum of the recoiling photofragments is equal in magnitude and opposite in direction to the rotational angular momentum of the C_2H_4OH radical product. This gives the usual classical expression:

$$\mu|\vec{v}_{rel}|b = I\omega \tag{3}$$

where b is the impact parameter, $\vec{v}_{rel}$ is the relative velocity between the Br and C_2H_4OH cofragments and $|\vec{v}_{rel}|$ is its magnitude, μ is the reduced mass of the C_2H_4OH + Br system, ω is the angular velocity of the rotating C_2H_4OH radicals, and I is the moment of inertia about the axis of rotation of the C_2H_4OH radical. In a simple impulsive model where the repulsive force acts along the direction of the C−Br bond, the axis of rotation is perpendicular to the plane containing the center of mass of the C_2H_4OH portion of the molecule, the Br atom, and the C atom bonded to the Br. Equation 3 leads to the prediction below for the rotational energy, E_R, imparted to the C_2H_4OH radical as a function of the measured recoil kinetic energy E_T:

$$E_R = \frac{\mu b^2}{I} E_T \tag{4}$$

If the equilibrium geometry of the radical product is significantly different from the geometry of the C_2H_4OH moiety of 2-bromoethanol, then both the moment of inertia and E_R will change while the angular momentum remains constant. Thus, our model continues by assuming this change in geometry is negligible. The success of this model relies on the fact that the excited state accessed at 193 nm is repulsive in the Franck−Condon region, so the impulsive model is reasonable.

The key new feature in this model is the calculation of the range of impact parameters the molecule accesses in both the zero-point vibrational wave function and in low lying vibrational quantum states, rather than using only the electronic minimum geometry. We first identify the harmonic normal modes that significantly affect the factor $\mu b^2/I$ by calculating the factor at 40 displacements from the equilibrium geometry along each normal mode, extending beyond the classical turning point. (The Gaussian output of the B3LYP/6-311++G(3df,2p) frequency calculation provides the displacement vectors of each atom for each normal vibrational mode.) In both T conformers of 2-bromoethanol, only the mode affecting the C−C−Br angle significantly altered the rotational energy partitioning; these are the harmonic modes with frequencies of 217.8 cm^{-1} (ν_3) and 210.8 cm^{-1} (ν_2) for the Tt and Tg conformers, respectively. Our model is greatly simplified by the fact that normal mode vibrations that displace primarily the H atoms need not be explicitly included, as they do not affect the rotational energy partitioning.

We calculate the probability density of a 2-bromoethanol molecule dissociating with a particular $\mu b^2/I$ factor in eq 3 from the square of the harmonic oscillator wave function at the displacement that gives the corresponding impact parameter and moment of inertia. This weighting generates a distribution of energies that is imparted to rotation for each measured recoil kinetic energy in the C−Br fission (as well as the corresponding J-distribution of the nascent radicals). We repeat the prediction of the distribution of energies imparted to rotation for C_2H_4OH radicals formed from 2-bromoethanol precursors with one and two quanta in the 217.8 cm^{-1} mode, again using the harmonic oscillator wave function for each quantum level.

D.2. Determining the Vibrational Energy Distribution of the C_2H_4OH Radicals. To validate our model, we use conservation of energy (eq 2) and the distribution of energies partitioned to rotation at each E_T to obtain the vibrational energy distribution of nascent C_2H_4OH radicals. This allows us to predict the portion of the $P(E_T)$ that would produce radicals that are stable to subsequent dissociation in section D.3. As in section B, we assume that the supersonic expansion rotationally cools the parent molecules and that they have a thermal distribution of vibrational energy at the nozzle temperature. However, instead of simply using an average internal energy for all parent molecules, we use a thermal distribution of vibrational energies in 2-bromoethanol. At each measured E_T, we thus account for both the range of rotational energies of the C_2H_4OH radicals and also the range of internal energies of the 2-bromoethanol photolytic precursor. For example, if the C−Br fission imparts 38 kcal/mol to E_T and results in a $Br(^2P_{3/2})$ cofragment, eq 2 predicts that 2-bromoethanol molecules with $E_{int}(CH_2BrCH_2OH)$ = 2 kcal/mol form C_2H_4OH radicals with a total internal energy of 42.53 kcal/mol. If these 2-bromoethanol molecules dissociate from a trans geometry, 97% do so with a $\mu b^2/I$ factor ranging from 0.60 to 0.34, which corresponds to a distribution of vibrational energies ranging from 20.11 to 29.61 kcal/mol. We weight the prediction for each E_T by the measured recoil kinetic energy distribution in Figure 2 and account for the thermal distribution of vibrational energies in the photolytic precursor. This gives a $P(E_{vib})$ for the radicals formed in the $Br(^2P_{3/2}) + C_2H_4OH$ dissociation channel. We then repeat the calculation for radicals formed in the $Br(^2P_{1/2}) + C_2H_4OH$ dissociation channel and sum the two to get the total distribution of vibrational energies in the nascent radicals.

D.3. Validating the Rotational Model by Predicting the Br + Stable C_2H_4OH $P(E_T)$. We validate this model by predicting the total recoil kinetic energy of Br + stable radicals and comparing it to the measured $P(E_T)$ for Br + stable radicals shown in Figure 6a. Figure 8 shows the increasing level of accuracy of the predicted $P(E_T)$ spectrum for Br + stable radicals as the model increases in sophistication. For each E_T there is a minimum amount of energy that must be partitioned to rotation to result in a stable C_2H_4OH radical (one with vibrational energy less than the 26.4 kcal/mol, the theoretically predicted dissociation barrier to OH + ethene). The predicted $P(E_T)$ spectrum is generated by calculating the percent of radicals formed with a given E_T that have E_{vib} below 26.4 kcal/mol. We do the calculation separately for the $Br(^2P_{3/2}) + C_2H_4OH$ and the $Br(^2P_{1/2}) + C_2H_4OH$ channels, and then sum these contributions. Frame a of Figure 8 shows the predicted $P(E_T)$ for Br + stable radicals if we only consider dissociation from the equilibrium geometry of the Tt conformer of 2-bromoethanol and use an average $E_{int}(CH_2BrCH_2OH)$ = 2.21 kcal/mol. Molecules with E_T = 36.9 kcal/mol formed in conjunction with $Br(^2P_{3/2})$ have an E_{vib} of exactly 26.4 kcal/mol if we only consider the impact parameter at the equilibrium geometry. Molecules with E_T greater than 36.9 kcal/mol will have an E_{vib} less than 26.4 and will thus be stable. Figure 8a clearly shows that consideration of only the equilibrium geometry and an average internal energy of the precursor does not adequately predict the measured spectrum of stable radicals. Frame b of Figure 8 shows the $P(E_T)$ for Br + stable radicals when 2.21 kcal/mol is taken as the average $E_{int}(CH_2BrCH_2OH)$ and the rotational model includes zero-point motion in the normal mode with a harmonic frequency corresponding to 217.8 cm^{-1}. (Including the simultaneous displacement along the second most important vibrational mode for rotational energy partitioning, the 1011.8 cm^{-1} mode of the Tt conformer, did not significantly alter the predicted spectrum. The prediction from the Tg conformer was nearly identical to that from the Tt conformer.) For each E_T, the fraction of nascent radicals that remains stable is the integral of the corresponding vibrational energy distribution from 0 to 26.4 kcal/mol. Frame c of Figure 8 includes both vibrational motion along the zero-point level and allows for a range of internal energies of the Tt conformer of 2-bromoethanol, as described in section D.2. The agreement in the region near E_T = 40 kcal/mol, the onset region for radical dissociation, is excellent, while the agreement throughout the entire Br + stable radical spectrum shows improvement. Frame d extends the model even further by individually considering 2-bromoethanol molecules in eigenstates with 0, 1, and 2 quanta in the ν_3 = 217.8 cm^{-1} normal mode. The resulting distributions of vibrational energy for each E_T are calculated using the square of the corresponding harmonic oscillator wave function. The distribution of internal energy in the precursor $E_{int}(CH_2BrCH_2OH)$ is still obtained from a thermal distribution, but we now explicitly incorporate the differing contribution to the internal energy for the eigenstates with 0, 1, or 2 quanta in the 217.8 cm^{-1} mode. Figure 8d shows the effect of increasing quanta in the ν_3 normal mode on the predicted spectrum for the stable radicals; the v = 2 state shows the largest range of energies imparted to rotational energy, resulting in a broader spectrum of stable radicals. The three predicted stable radical $P(E_T)$ spectra were added to get the total predicted stable radical $P(E_T)$ spectrum shown as a red dashed line in Figure 8d. (We assume that 2-bromoethanol molecules with more than 2 quanta in the 217 cm^{-1} mode give stable radicals with a distribution similar to the v = 2 prediction.) Notice the further improved

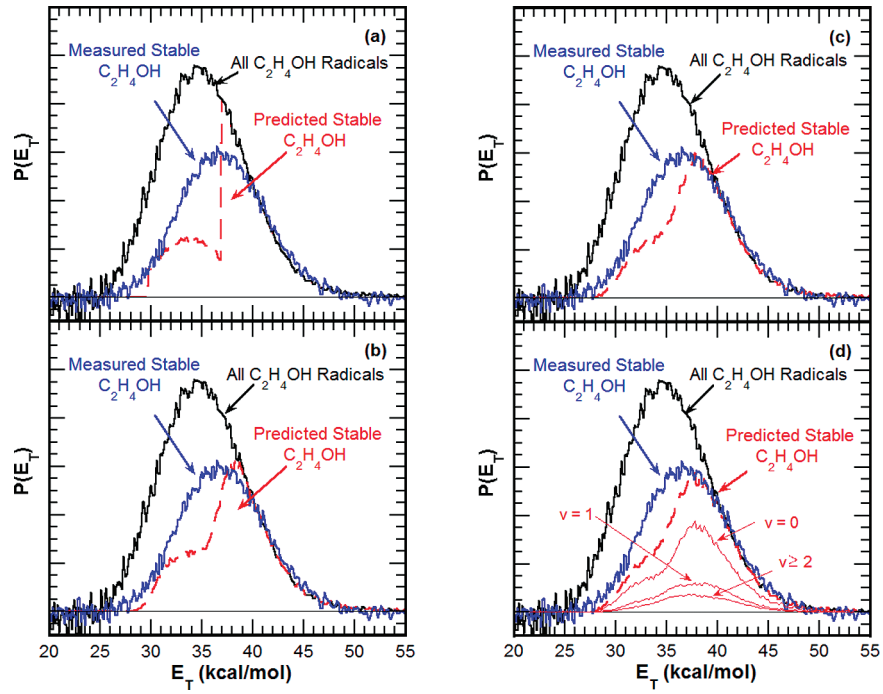

Figure 8. Progression of the predicted $P(E_T)$ distribution for the production of stable C_2H_4OH + Br (red dashed line) as we modify an impulsive model for the rotational energy partitioning during the photodissociation of the Tt conformer of 2-bromoethanol. Also shown for comparison is the measured stable C_2H_4OH + Br $P(E_T)$ (blue solid line) and the $P(E_T)$ for the production of all nascent radicals + Br as a black solid line from Figure 6a. The impulsive model in each plot uses the measured $P(E_T)$ for all nascent radicals + Br and (a) the equilibrium geometry of the Tt conformer and an average $E_{int}(CH_2BrCH_2OH) = 2.21$ kcal/mol, (b) the range of geometries accessed from zero-point motion along the 217.8 cm^{-1} normal mode of the Tt conformer and an average $E_{int}(CH_2BrCH_2OH) = 2.21$ kcal/mol, (c) the geometries accessed from zero-point motion along the 217.8 cm^{-1} normal mode of the Tt conformer and a thermal distribution of $E_{int}(CH_2BrCH_2OH)$, and (d) the distribution of internal energies and geometries accessed from motion along vibrational eigenstates with 0, 1, and 2 quanta in the 217.8 cm^{-1} mode of the Tt conformer. The contribution from eigenstates with 0 and 1 quanta in this mode are weighted by their thermal population at 345.15 K, 59.5% and 24.1%, respectively. The contribution from eigenstates with more than 2 quanta in this mode is assumed to be similar to the contribution from eigenstates with 2 quanta, and thus this contribution is weighted by the remaining 16.4%. As the impulsive model for rotational energy partitioning is refined to include the internal energy distribution and vibrational eigenstates of the photolytic precursor, the predicted stable radical $P(E_T)$ converges more and more closely to the experimentally determined $P(E_T)$ for stable C_2H_4OH radicals + Br.

agreement between the predicted and measured stable radical distributions. Note that all frames in Figure 8 show the resulting prediction for the spectrum of stable radicals assuming the 2-bromoethanol molecules dissociate from a trans geometry about the C−C bond.

One surprising result from this model is the poor prediction for the stable radical spectrum when the Gg conformer of 2-bromoethanol is used as the photolytic precursor, as shown in the Supporting Information. The Gg conformer is the lowest in energy, and the G4 energetics predict that a thermal population of 2-bromoethanol at the nozzle temperature should comprise 78% of Gg molecules. This conformer has a gauche relation between the C−OH and C−Br bonds with a dihedral angel of ~60° and a considerably larger impact parameter than the trans conformers. (At the equilibrium geometry of the Gg conformer, $b = 1.3$ Å, $I = 52.5$ amu Å^2, and $E_R = 0.93E_T$.) If C−Br bond fission occurred primarily from this geometry, we predict that virtually all of the radicals across the E_T distribution would form with substantial rotational energy and remain stable to subsequent dissociation. This is inconsistent with the measured distribution for stable C_2H_4OH radicals. (It is possible that a small fraction of the gauche conformers undergo HBr elimination rather than C−Br bond fission. Though electron bombardment ionization measurements do not detect any signal at HBr^+ (see the Supporting Information), recent single photon ionization measurements at 15.34 eV reveal a signal that is 2.5% that of the Br atom signal at the same photoionization energy.[90]) If we assume that a substantial fraction of the gauche 2-bromoethanol molecules isomerizes to a trans geometry on the excited state before dissociating, then we can fit the measured stable radical spectrum quite well. Figure 9 shows the predicted stable radical spectrum assuming that three-fourths of all the thermal gauche ground state molecules isomerize to a trans geometry in the excited state; thus the prediction assumes that 20% of the 2-bromoethanol molecules dissociate from a gauche geometry and 80% have a trans geometry upon accessing the repulsive region of the excited state potential.

V. Discussion

The bimolecular reaction of OH with ethene is believed to be a significant source of ethenol in flames, but the mechanism of its production is not well understood. An intensive study of the temperature dependent product branching would provide valuable insight to this system. Combustion models tend to include only the direct abstraction reaction of OH + ethene to yield H_2O + vinyl. However, at lower temperatures the addition channel becomes increasingly important. To access the critical portions of the potential energy surface for product branching from the addition reaction, we use a photolytic precursor to generate the first radical intermediate in a range of vibrational energies spanning the barrier heights of interest. Photolytic precursors for the 2-hydroxyethyl intermediate have presented challenges as 2-chloroethanol has a low absorption cross-section, 2-bromoethanol and 2-iodoethanol partition a significant amount of energy into the rotation of the C_2H_4OH photofragment, and

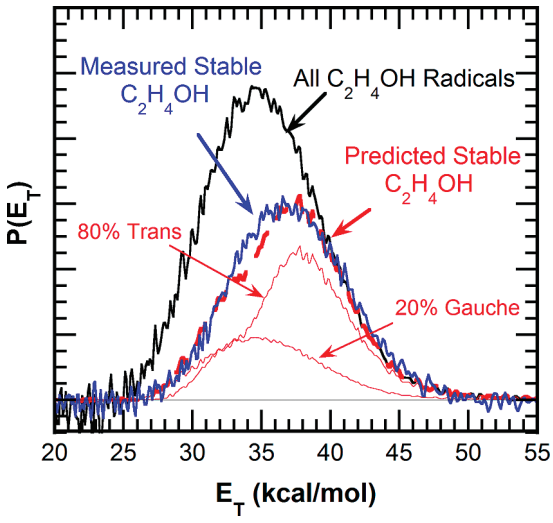

Figure 9. Predicted $P(E_T)$ for stable C_2H_4 OH radicals + Br assuming 20% of the photolytic precursors dissociate from a gauche geometry (the Gg conformer) and 80% dissociate from a trans geometry (39.5% from the Tt conformer and 40.5% from the Tg conformer). The contribution from each conformer includes the internal energy distribution and range of geometries in the vibrational eigenstates with 0, 1, and 2 quanta in the most significant vibrational normal mode (217.8 cm^{-1} for Tt, 210.9 cm^{-1} for Tg, and 257.7 cm^{-1} for Gg).

2-iodoethanol generates primarily stable radicals at the wavelengths studied thus far. In this work, we develop a model for the rotational energy partitioning to the C_2H_4OH radical from the photodissociation of 2-bromoethanol at 193 nm to make it a useful photolytic precursor for the study of the product branching channels on the OH + ethene potential energy surface. Using our rotational model to determine an accurate vibrational energy distribution for the nascent radicals in our experiment allows us to predict the branching to each of the energetically allowed product channels of the C_2H_4OH reaction intermediate by averaging over the microcanonical rate constants. These can be directly compared to the measured branching fractions to each of these product channels in an experiment where the 2-hydroxyethyl radical intermediate is generated from this photolytic precursor. Such a comparison is important in establishing the accuracy of the statistical microcanonical rate constants used to predict the product branching as a function of temperature and pressure for the OH + ethene reaction in bulk kinetics modeling of combustion.[19]

We improve upon previous attempts to model the rotational energy partitioning to the C_2H_4OH radical by using our experimentally measured translational energy distribution (rather than one predicted by an impulsive model) and conservation of angular momentum while including the range of geometries accessed by the vibrations of the photolytic precursor. In contrast, prior work[60] assumed a semirigid radical dissociation from the equilibrium geometry of the lowest energy conformer to calculate a single average rotational energy. Our modeling also provides convincing evidence that a significant portion of the lowest energy conformer of 2-bromoethanol, the Gg conformer, undergoes isomerization to a trans configuration about the C−C bond on the excited state prior to accessing the repulsive region of the potential energy surface. By selectively detecting the spin−orbit states of Br, this work has also resolved the two sources of stability for the C_2H_4OH fragments: those that are stable by virtue of 10.54 kcal/mol being partitioned to the $Br(^2P_{1/2})$ cofragment and those that are stable due to a large partitioning of the internal energy to rotation. Thus we fully

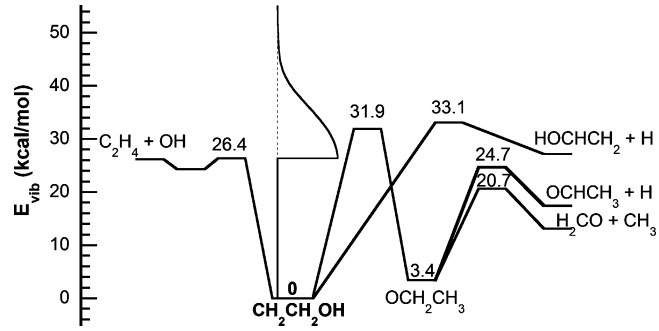

Figure 10. Vibrational energy distribution derived for unstable C_2H_4OH radicals from the same model used to predict the Br + stable radical $P(E_T)$ in Figure 9. The distribution is superimposed on some of the more important transition states and product channels of the OH + ethene reaction as calculated by Senosiain et al.[19]

characterize these two potential sources of stability, both of which were considered in the early work of Lee and coworkers.[58]

Our model for the partitioning of the internal energy of the C_2H_4OH photofragment into rotation gives a good fit to the measured translational energy distribution for the stable portion of the nascent radicals if we assume that 80% of the 2-bromoethanol molecules dissociate from a trans conformer and 20% from a gauche geometry about the C−C bond. Including both the distribution of internal energy and motion along one of the vibrational modes of the Tt conformer (Figure 8d) gives excellent agreement in the onset region for dissociation of the nascent radicals. Using this same model for the other 2-bromoethanol conformers and weighting the resulting predictions for 80% trans and 20% gauche, we calculated the vibrational energy distribution of the nascent C_2H_4OH radicals formed from the photodissociation of 2-bromoethanol at 193 nm. Figure 10 shows the vibrational energy distribution of the radicals with $E_{vib} \geq 26.4$ kcal/mol, the OH + ethene asymptote, on portions of the potential energy surface calculated by Senosiain et al.[19] The vibrational energy distribution spans both the OH + ethene reactant asymptote and the predicted barrier to the H + ethenol product channel. We used the transition states calculated by Senosiain et al. and reported in Tables 2 and 3 of ref 19 to predict the branching between the product channels in the reaction of OH + ethene if the vibrational energy of the radical intermediate were that depicted in Figure 10. The RRKM microcanonical rate constants predict that 99.7% of the radicals would dissociate to OH + ethene; this corresponds to the inelastic collisions in an OH + ethene bimolecular reaction. Of the reactive portion, 58% result in H + ethenol products, 39% result in $H_2CO + CH_3$ products, and 3% result in H + acetaldehyde. Though the vibrational energy distribution does not correspond to a thermal one, it is well characterized, and so offers a definitive benchmark for the theoretical predictions of the product branching in this system. The predicted branching fractions above do not include a correction for H atom tunneling through the $C_2H_4OH \rightarrow OCH_2CH_3$ barrier; tunneling must be included to accurately predict the branching fraction to the $H_2CO + CH_3$ and H + acetaldehyde product channels.[19]

The computational work of Senosiain et al.[19] permits a prediction for the OH + ethene product branching as a function of total angular momentum, J, of the C_2H_4OH radical. As J increases with the total internal energy of the radical constant, one expects the ratio of the partial cross-section for the H + ethenol product channel to the partial cross-section for the $H_2CO + CH_3$ product channel to decrease because the $H_2CO + CH_3$ channel has the lower calculated barrier. (When the total

vibrational energy is near the H + ethenol barrier, the rate constant to $H_2CO + CH_3$ is still substantial.) To illustrate this effect, we calculate how the predicted branching above compares to the predicted branching if all the internal energy were in vibrational energy of the radicals (the low *J* limit). Then the reactive portion would result in 71% H + ethenol products and 24% $H_2CO + CH_3$ products. The model for the rotational energy partitioning also allows us to predict how the branching fraction of the H + ethenol channel would change as a function of the total recoil kinetic energy in the primary photodissociation. Our ongoing work on this system seeks to test the microcanonical rate constants predicted by the theoretical transition states by detecting the velocity distribution of the ethenol products. The change in relative branching to the ethenol product channel as a function of translational energy imparted in the primary photodissociation gives an experimental measurement of the change in the average microcanonical product branching to this channel as a function of internal energy. We can also investigate the branching to the other product channels, including acetaldehyde + H and $CH_3 + H_2CO$ accessed via isomerization to OCH_2CH_3.

This work also measures the angular distribution of the Br atom photofragments from 2-bromoethanol photodissociation. Beginning with studies by van Veen et al.,[91] studies of the photodissociation alkyl bromides have produced $Br(^2P_{1/2})$ atoms from excitation from the ground state to the $^3Q_0$ state via a parallel transition and $Br(^2P_{3/2})$ atoms from excitation to the $^1Q_1$ state via a perpendicular transition at higher photodissociation energies. Our measured anisotropy parameters for Br atoms from the photodissociation of 2-bromoethanol at 193 nm are more isotropic than the strongly parallel and perpendicular anisotropies derived for bromomethane but retain the feature that $Br(^2P_{1/2})$ results from absorption via a transition moment parallel to the C−Br bond where $Br(^2P_{3/2})$ for a transition moment perpendicular to the C−Br bond. This is also in accord with the angular distributions that Chandler et al.[59] observed for bromomethane and 2-bromoethanol, and also Lee and co-workers' suggestion that isomerization in the excited state can reduce the measured anisotropies.

Acknowledgment. The Department of Energy, Basic Energy Sciences, supported this work under award number DE-FG02-92ER14305. Additional support was provided by the University of Chicago and the Department of Energy under H.44 of the Department of Energy Contract No. DE-AC02-07CH11359 awarded to Fermi Research Alliance LLC. A National Science Foundation Graduate Research Fellowship supported B.R. We extend our gratitude to our co-worker, Bridget Alligood, for taking the HBr spectrum that is shown in the Supporting Information. We also thank Christopher Clark (Carleton College) and Daniel Simmons-Marengo (University of Chicago Laboratory School) for their assistance both with the experiment and recoding the program to calculate the rotational energy partitioning predicted from a given precursor geometry.

Supporting Information Available: B3LYP/6-311++G(3df,2p) equilibrium geometries, rotational constants, unscaled harmonic vibrational frequencies, zero-point corrections, displacement vectors for significant normal modes of vibration, and G4 energies for the conformers of 2-bromoethanol and the 2-hydroxyethyl radical. Figures of the velocity distribution of m/e = 45, time-of-flight distributions of m/e = 79 and 81 from the scattering experiments, and the predicted $P(E_T)$ of Br + stable C_2H_4OH radicals when photodissociation occurs from the Gg conformer of 2-bromoethanol. Figures and analysis of the angular distribution of the photofragments detected in this study. This material is available free of charge via the Internet at http://pubs.acs.org.

References and Notes

(1) Cool, T. A.; Nakajima, K.; Mostefaoui, T. A.; Qi, F.; McIlroy, A.; Westmoreland, P. R.; Law, M. E.; Poisson, L.; Peterka, D. S.; Ahmed, M. *J. Chem. Phys.* **2003**, *119*, 8356.
(2) Taatjes, C. A.; Hansen, N.; McIlroy, A.; Miller, J. A.; Senosiain, J. P.; Klippenstein, S. J.; Qi, F.; Sheng, L.; Zhang, Y.; Cool, T. A.; Wang, J.; Westmoreland, P. R.; Law, M. E.; Kasper, T.; Kohse-Höinghaus, K. *Science* **2005**, *308*, 1887.
(3) Taatjes, C. A.; Hansen, N.; Miller, J. A.; Cool, T. A.; Wang, J.; Westmoreland, P. R.; Law, M. E.; Kasper, T.; Kohse-Höinghaus, K. *J. Phys. Chem. A* **2006**, *110*, 3254.
(4) Calvert, J. G.; Atkinson, R.; Kerr, J. A.; Madronich, S.; Moortgat, G. K.; Wallington, T. J.; Yarwood, G. *The Mechanisms of Atmospheric Oxidation of the Alkenes*; Oxford University Press, Inc.: New York, 2000; Chapter 1.
(5) Sosa, C.; Schlegel, H. B. *J. Am. Chem. Soc.* **1987**, *109*, 4193.
(6) Sosa, C.; Schlegel, H. B. *J. Am. Chem. Soc.* **1987**, *109*, 7007.
(7) Villà, J.; Gonzàlez-Lafont, A.; Lluch, J. M.; Corchado, J. C.; Espinosa-Garcià, J. *J. Chem. Phys.* **1997**, *107*, 7266.
(8) Sekušak, S.; Liedl, K. R.; Sabljić., A. *J. Phys. Chem. A* **1998**, *102*, 1583.
(9) Caralp, F.; Devolder, P.; Fittschen, C.; Gomez, N.; Hippler, H.; Méreau, R.; Rayez, M. T.; Striebel, F.; Viskolez, B. *Phys. Chem. Chem. Phys.* **1999**, *1*, 2935.
(10) Hoyermann, K.; Olzmann, M.; Seeba, J.; Viskolcz, B. *J. Phys. Chem. A* **1999**, *103*, 5692.
(11) Yamada, T.; Bozzelli, J. W.; Lay, T. *J. Phys. Chem. A* **1999**, *103*, 7646.
(12) Hippler, H.; Viskolcz, B. *Phys. Chem. Chem. Phys.* **2000**, *2*, 3591.
(13) Alvarez-Idaboy, J.; Mora-Diez, N.; Vivier-Bunge, A. *J. Am. Chem. Soc.* **2000**, *122*, 3715.
(14) Piqueras, M. C.; Crespo, R.; Nebot-Gil, I.; Tomás, F. *THEOCHEM* **2001**, *527*, 199.
(15) Liu, G.; Ding, Y.; Li, Z.; Fu, Q.; Huang, X.; Sun, C.; Tang, A. *Phys. Chem. Chem. Phys.* **2002**, *4*, 1021.
(16) Zhang, Y.; Zhang, S.; Li, Q. *Chem. Phys.* **2005**, *308*, 109.
(17) Zhang, Y.; Zhang, S.; Li, Q. *Chem. Phys.* **2004**, *296*, 79.
(18) Zhu, R. S.; Park, J.; Lin, M. C. *Chem. Phys. Lett.* **2005**, *408*, 25.
(19) Senosiain, J. P.; Klippenstein, S. J.; Miller, J. A. *J. Phys. Chem. A* **2006**, *110*, 6960.
(20) Vakhtin, A. B.; Murphy, J. E.; Leone, S. R. *J. Phys. Chem. A* **2003**, *107*, 10055.
(21) Bradley, J. N.; Capey, W. D.; Fair, R. W.; Pritchard, D. K. *Int. J. Chem. Kinet.* **1976**, *8*, 549.
(22) Bott, J. F.; Cohen, N. *Int. J. Chem. Kinet.* **1991**, *23*, 1075.
(23) Frenklach, M.; Wang, H.; Rabinowitz, M. J. *Prog. Energy Combust. Sci.* **1992**, *18*, 47.
(24) Hidaka, Y.; Nishimori, T.; Sato, K.; Henmi, Y.; Okuda, R.; Inami, K.; Higashihara, T. *Combust. Flame* **1999**, *117*, 755.
(25) Bradley, J. N.; Hack, W.; Hoyerman, K.; Wagner, H. G. *J. Chem. Soc., Faraday Trans. 1* **1973**, *69*, 1889.
(26) Greiner, N. R. *J. Chem. Phys.* **1970**, *53*, 1284.
(27) Morris, E. D.; Stedman, D. H.; Niki, H. *J. Am. Chem. Soc.* **1971**, *93*, 3570.
(28) Davis, D. D.; Huie, R. E.; Herron, J. T. *J. Chem. Phys.* **1973**, *59*, 628.
(29) Smith, I. W. M.; Zellner, R. *J. Chem. Soc., Faraday Trans. 2* **1973**, *69*, 1617.
(30) Gordon, S.; Mulac, W. A. *Proc. Symp. Chem. Kinet. Data Upper Lower Atmos.* **1974**, 289.
(31) Atkinson, R.; Pitts, J. N. *J. Chem. Phys.* **1975**, *63*, 3591.
(32) Davis, D. D.; Fischer, S.; Schiff, R.; Watson, R. T.; Bollinger, W. *J. Chem. Phys.* **1975**, *63*, 1707.
(33) Pastrana, A. V.; Carr, R. W. *J. Phys. Chem.* **1975**, *79*, 765.
(34) Howard, C. J. *J. Chem. Phys.* **1976**, *65*, 4771.
(35) Lloyd, A. C.; Darnall, K. R.; Winer, A. M.; Pitts, J. N. *J. Phys. Chem.* **1976**, *80*, 789.
(36) Atkinson, R.; Perry, R. A.; Pitts, J. N. *J. Chem. Phys.* **1977**, *66*, 1197.
(37) Atkinson, R.; Perry, R. A.; Pitts, J. N. *J. Chem. Phys.* **1977**, *67*, 3170.
(38) Overend, R.; Paraskevopoulos, G. J. *J. Chem. Phys.* **1977**, *67*, 674.
(39) Farquharson, G. K.; Smith, R. H. *Aust. J. Chem.* **1980**, *33*, 1425.
(40) Atkinson, R.; Aschmann, S. M.; Winer, A. M.; Pitts, J. N. *Int. J. Chem. Kinet.* **1982**, *14*, 507.
(41) Tully, F. P. *Chem. Phys. Lett.* **1983**, *96*, 148.
(42) Atkinson, R.; Aschmann, S. M. *Int. J. Chem. Kinet.* **1984**, *16*, 1175.

(43) Klein, T.; Barnes, I.; Becker, K. H.; Fink, E. H.; Zabel, F. *J. Phys. Chem.* **1984**, *88*, 5020.
(44) Schmidt, V.; Zhu, G. Y.; Becker, K. H.; Fink, E. H. *Ber. Bunsen-Ges. Phys. Chem.* **1984**, *89*, 321.
(45) Zellner, R.; Lorenz, K. *J. Phys. Chem.* **1984**, *88*, 984.
(46) Atkinson, R. *Chem. Rev.* **1986**, *86*, 69.
(47) Liu, A.; Mulac, W. A.; Jonah, C. D. *Int. J. Chem. Kinet.* **1987**, *19*, 25.
(48) Liu, A. D.; Mulac, W. A.; Jonah, C. D. *J. Phys. Chem.* **1988**, *92*, 3828.
(49) Tully, F. P. *Chem. Phys. Lett.* **1988**, *143*, 510.
(50) Westbrook, C. K.; Thornton, M. M.; Pitz, W. J.; Malte, P. C. *Proc. Combust. Inst.* **1989**, *22*, 863.
(51) Nielson, O. J.; Jorgensen, O.; Donlon, M.; Sidebottom, H. W.; O'Farrell, D. J.; Treacy, J. *Chem. Phys. Lett.* **1990**, *168*, 319.
(52) Becker, K. H.; Geiger, H.; Wiesen, P. *Chem. Phys. Lett.* **1991**, *184*, 256.
(53) Diau, E.; Lee, Y. P. *J. Phys. Chem.* **1991**, *95*, 379.
(54) Kuo, C. H.; Lee, Y. P. *J. Phys. Chem.* **1991**, *95*, 1253.
(55) Diau, E. W.; Lee, Y. P. *J. Chem. Phys.* **1992**, *96*, 377.
(56) Fulle, D.; Hamann, H. F.; Hippler, H.; Jansch, C. P. *Ber. Bunsen-Ges. Phys. Chem.* **1997**, *101*, 1433.
(57) Chuong, B.; Stevens, P. S. *J. Phys. Chem. A* **2000**, *104*, 5230.
(58) Hintsa, E. J.; Zhao, X.; Lee, Y. T. *J. Chem. Phys.* **1990**, *92*, 2280.
(59) Chandler, D. W.; Thoman, J. W.; Hess, W. P. *Inst. Phys. Conf. Ser.* **1990**, No. 114, 355
(60) Sapers, S. P.; Hess, W. P. *J. Chem. Phys.* **1992**, *97*, 3126.
(61) Shubert, V. A.; Rednic, M.; Pratt, S. T. *J. Phys. Chem A* **2009**, *113*, 9057.
(62) Hippler, H.; Viskolcz, B. *Phys. Chem. Chem. Phys.* **2000**, *2*, 3591.
(63) Cleary, P. A.; Baeza Romero, M. T.; Blitz, M. A.; Heard, D. E.; Pilling, M. J.; Seakins, P. W.; Wang, L. *Phys. Chem. Chem. Phys.* **2006**, *8*, 5633.
(64) Hippler, H.; Klinger, M.; Strasteva, N.; Nasterlack, S.; Olzmann, M.; Striebel, F. Proceedings of the European Combustion Meeting 2005.
(65) Bartels, M.; Hoyermann, K.; Sievert, R. *Proc. Combust. Inst.* **1982**, *19*, 61.
(66) Buckley, P.; Giguere, P.; Schneider, M. *Can. J. Chem.* **1969**, *47*, 901.
(67) Homanen, L. *Spectrochim. Acta* **1983**, *39A*, 77.
(68) Hagen, K.; Hedberg, K. *J. Am. Chem. Soc.* **1973**, *95*, 8263.
(69) Huang, J.; Hedberg, K. *J. Am. Chem. Soc.* **1989**, *111*, 6909.
(70) Thomassen, H.; Samdal, S.; Hedberg, K. *J. Phys. Chem.* **1993**, *97*, 4004.
(71) Almenningen, A.; Bastiansen, O.; Fernhold, L.; Hedberg, K. *Acta Chem. Scand.* **1973**, *25*, 1946.
(72) Almenningen, A.; Fernholt, L.; Kveseth, K. *Acta Chem. Scand.* **1977**, *A31*, 297.
(73) Buckton, K. S.; Azrak, R. G. *J. Chem. Phys.* **1970**, *52*, 5652.
(74) Azrak, R. G.; Wilson, E. B. *J. Chem. Phys.* **1970**, *52*, 5299.
(75) Heck, A. J. R.; Chandler, D. W. *Annu. Rev. Phys. Chem.* **1995**, *46*, 335.
(76) Eppink, A. T. J. B.; Parker, D. H. *Rev. Sci. Instrum.* **1997**, *68*, 3477.
(77) Sato, Y.; Matsumi, Y.; Kawasaki, M.; Tsukiyama, K.; Bersohn, R. *J. Phys. Chem.* **1995**, *99*, 16307.
(78) Liu, Y.; Butler, L. J. *J. Chem. Phys.* **2004**, *121*, 11016.
(79) Lau, K.-C.; Liu, Y.; Butler, L. J.; Lin, J. J. *J. Chem. Phys.* **2006**, *125*, 144312.
(80) Chang, B.; Hoetzlein, R. C.; Mueller, J. A.; Geiser, J. D.; Houston, P. L. *Rev. Sci. Instrum.* **1998**, *69*, 1665.
(81) Curtiss, L. A.; Redfern, P. C.; Raghavachari, K.; Pople, J. A. *J. Chem. Phys.* **2001**, *114*, 108.
(82) Curtiss, L. A.; Redfern, P. C.; Raghavachari, K. *J. Chem. Phys.* **2007**, *126*, 084108.
(83) Frisch, M. J.; Trucks, G. W.; Schegel, H. B.; et al. *Gaussian 09*, Revision A.02, Gaussian, Inc.: Wallingford, CT, 2009.
(84) Dribinski, V.; Ossadtchi, A.; Mandelshtam, V. A.; Reisler, H. *Rev. Sci. Instrum.* **2002**, *73*, 2634.
(85) Moore, C. E. *Atomic Energy Levels* **1971**, *II*, 159 NSRDS-NBS 35.
(86) Tang, X. N.; Ratliff, B. J.; FitzPatrick, B. L.; Butler, L. J. *J. Phys. Chem. B* **2008**, *112*, 16050.
(87) Ratliff, B. J.; Tang, X. N.; Butler, L. J.; Szpunar, D. E.; Lau, K.-C. *J. Chem. Phys.* **2009**, *131*, 044304.
(88) Riley, S. J.; Wilson, K. R. *Faraday Discuss. Chem. Soc.* **1972**, *53*, 132.
(89) Szpunar, D. E. *Centrifugal Effects in the Dissociation Dynamics of Allyl Iodide and Rotationally Excited Allyl Radicals*; University of Chicago, Chicago, IL, 2003; Appendix C.
(90) Ratliff, B. J.; Alligood, B. W.; Butler, L. J.; Lee, S.-H. Lin, J. J. Manuscript in preparation.
(91) Van Veen, G. N. A.; Baller, T.; De Vries, A. E. *Chem. Phys.* **1985**, *92*, 59.

JP911739A